PSFC/RR-08-11

Role of zonal flows in trapped electron mode turbulence through nonlinear gyrokinetic particle and continuum simulation

Ernst, D. R.; Lang, J.[1]; Nevins, W. M.[2]; Hoffman, M.[3];
Chen, Y.[1]; Dorland, W.[4]; Parker, S.[1]

[1]University of Colorado, Boulder
[2]Lawrence Livermore National Laboratory
[3]Missouri University of Science and Technology
[4]University of Maryland

Plasma Science and Fusion Center
Massachusetts Institute of Technology
Cambridge MA 02139 USA

This work was supported in part by the U.S. Department of Energy, Grant No. DE-FG02-91ER-54109.

Role of Zonal Flows in TEM Turbulence through Nonlinear Gyrokinetic Particle and Continuum Simulation

D. R. Ernst 1), J. Lang 2), W. Nevins 3), M. Hoffman 4), Y. Chen 2), W. Dorland 5), S. Parker 2)

1) Plasma Science and Fusion Center, Mass. Inst. of Technology, Cambridge, MA, USA
2) Dept. of Physics, Univ. Colorado, Boulder, CO, USA
3) Lawrence Livermore National Laboratory, Livermore, CA, USA
4) Dept. of Nuclear Engineering, Univ. Missouri, Rolla, MO, USA
5) Dept of Physics, IREAP & CSCAMM, Univ. Maryland, College Park, MD, USA

e-mail contact of main author: dernst@psfc.mit.edu

Abstract. Trapped electron mode (TEM) turbulence exhibits a rich variety of collisional and zonal flow physics. This work explores the parametric variation of zonal flows and underlying mechanisms through a series of linear and nonlinear gyrokinetic simulations, using both particle-in-cell (the GEM code) and continuum (the GS2 code) methods. The two codes are shown to closely agree except at the largest values of $\eta_e = d\ln T_e/d\ln n_e \geq 5$, where qualitative agreement is found. A new stability diagram for electron modes is presented, identifying $\eta_e = 1$ as a critical boundary separating long and short wavelength TEMs. A scan of η_e shows fine scale structure appears when $\eta_e \gtrsim 1$, consistent with linear expectations. Zonal flows are weak when η_e exceeds unity. For $\eta_e > 1$, transport levels fall inversely with a power law in η_e. For $\eta_e \gg 1$, bispectral analysis supports a simple analytic model in which the dominant primary mode couples to itself to drive zonal fluctuations.

1. Introduction

Trapped electron mode turbulence is relevant to particle and electron thermal energy transport. Several types of TEM exist, driven by either the electron density gradient, or by the electron temperature gradient. The most significant modes are associated with non-resonant "bad curvature" drive as well as toroidal precession drift resonance. TEM turbulence is most relevant when toroidal ITG modes are either stable or weakly unstable. This scenario arises in a variety of contexts, such as internal transport barriers, cases with strong density peaking, cases with $T_e > T_i$, and low density regimes in which confinement scales favorably with density. Understanding of the mechanisms underlying particle and electron thermal energy transport could impact future devices such as ITER, where core fueling is greatly reduced, and electrons are heated directly by α-particles. In Alcator C-Mod ITB plasmas, TEM turbulence produces strong particle and electron

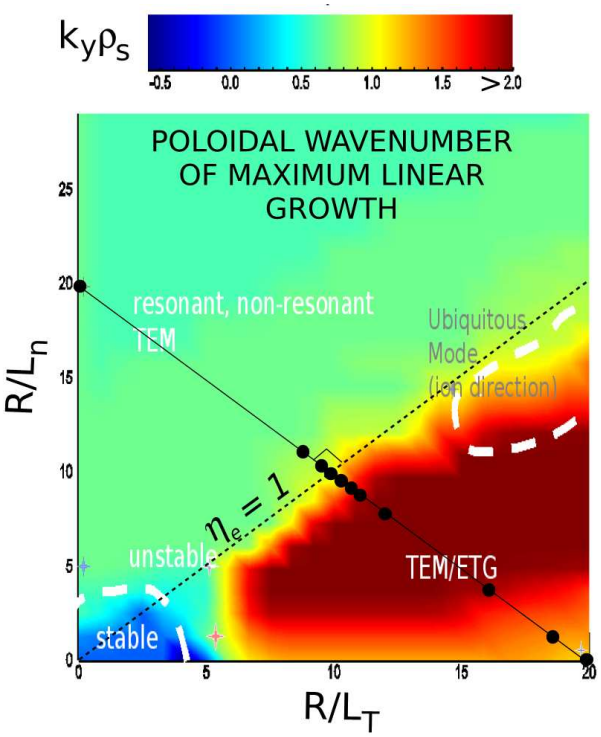

FIG. 1. Most unstable poloidal wavenumber $k_y\rho_s$ for electron modes, showing sudden onset of short wavelengths for $\eta_e > 1$. The η_e values chosen for the nonlinear scan lie on a line normal to $\eta_e = 1$.

thermal energy transport as the density gradient, and the electron temperature increase, which allows internal transport barriers to be controlled externally by ICRH [1, 2]. TEM turbulence is of particular interest in scenarios with primarily electron heating [3, 4]. Nonlinear gyrokinetic simulations of TEM turbulence have closely reproduced the measured wavelength spectrum of density fluctuations in an ITB experiment in which TEMs were predicted to be the dominant instability [2, 5], in a first of kind comparison.

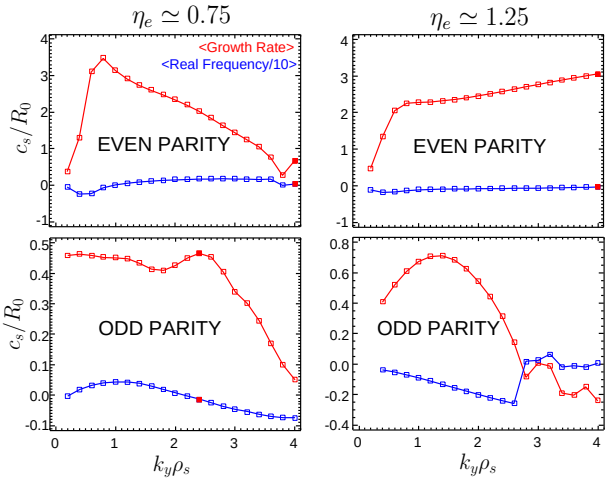

FIG. 2. Odd parity modes are much weaker than even parity modes, suggesting that TEMs, rather than ETG modes, are dominant over the wavelength range considered.

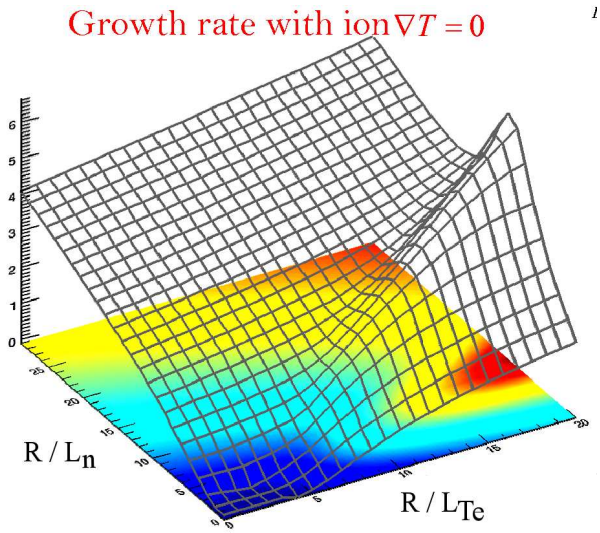

FIG. 3. Maximum linear growth rate as a function of R/L_{Te} and R/L_n, in units of c_s/R_0.

Recent work on TEM turbulence resulted in an apparent contradiction regarding the role of zonal flows. Initial studies revealed a new nonlinear upshift of the TEM critical density gradient [1], in which zonal flows were clearly important. In these purely density gradient driven cases, the role of secondary instability is evident in the creation of zonal flow dominated, quasi-steady states in the upshift regime. The upshift increases strongly with collisionality [2], consistent with the strong damping of TEMs by electron detrapping, and the relatively weak ion collisional damping of zonal flows. In contrast, zonal flows were shown to have little effect on the TEM saturation level in cases with strong electron temperature gradients and $T_e = 3T_i$ [6]. This apparent contradiction was resolved by work that bridged the two regimes [7, 8]. The importance of zonal flows in TEM turbulence was found to depend on ∇T_e and T_e/T_i [7]. The role of zonal flows in saturating TEM turbulence is consistent with the ratio of the zonal flow $E \times B$ shearing rate to the maximum linear growth rate [7, 9]. When zonal flows are not the dominant saturation mechanism, a simple mode coupling model shows that otherwise stable density fluctuations, with poloidal wavenumbers $k_y = 0$, are driven to large amplitudes at twice the growth rate of the dominant "primary" mode [9]. Simple estimates of the saturation level are obtained from the mode coupling model by setting the nonlinear growth rate to zero. Agreement is obtained with the GEM simulations in the early phase of saturation [9].

To establish a connection between zonal flows and plasma parameters, we begin with a detailed linear stability analysis of electron modes. The results of this stability analysis suggest η_e is an important parameter with a critical value near unity. Based on the linear results, we construct a scan of η_e along a line normal to $\eta_e = 1$, with fine increments where rapid changes in the linear spectrum are observed (see Fig. 1). We consider the "Cyclone Base Case" [10], idealized

from a DIII-D L-Mode plasma. To study electron modes and avoid ITG modes, we zero the ion temperature gradient for all cases, and scan the electron temperature and density gradients. Other parameters are held fixed at $T_e = T_i$, $\hat{s} = r/q\,dq/dr = 0.8$, $r/R0 = 0.18$, $q = 1.4$, $\beta = 0$, deuterium ions, real electron mass, circular concentric geometry, and collisionless.

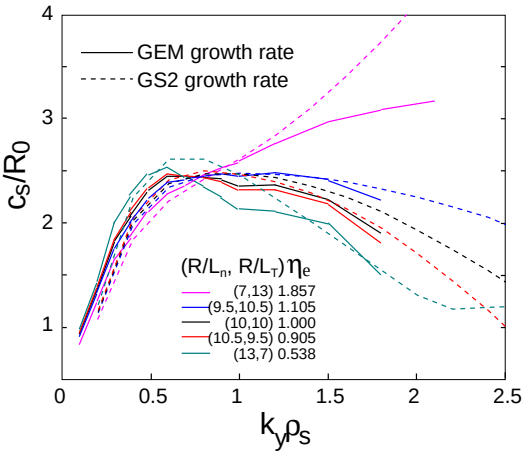

FIG. 4. Comparison of linear growth rate spectra from GEM and GS2 for the Cyclone case in hydrogen.

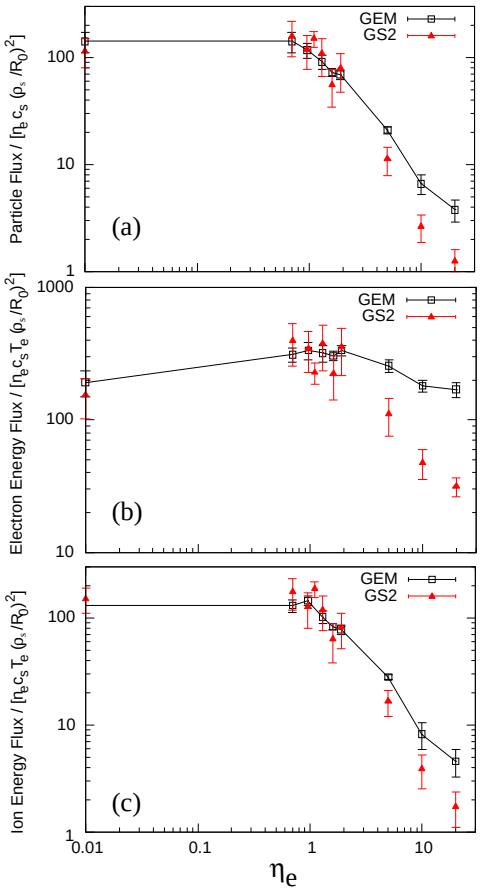

FIG. 5. Comparison of fluxes. Error bars represent standard deviation. (a) Particle flux (b) Electron energy flux (c) Ion energy flux.

2. Linear Stability Analysis

Using over 2,000 linear GS2 simulations, each sweeping the poloidal wavenumber $0 < k_y\rho_s < 4$, we have constructed a new and detailed stability diagram for electron modes as a function of their driving gradients, keeping zero ion temperature gradient. Here $\rho_s = c_s/\Omega_i$ with sound speed $c_s^2 = T_e/m_i$ and Ω_i the ion cyclotron frequency. Figure 1 shows the poloidal wavenumber of maximum growth as a function of the driving factors, the inverse gradient scale lengths for density and temperature, $R/L_n = -Rd\ln n/dr$ and $R/L_{Te} = -Rd\ln T_e/dr$, where (R,r) is the (major, minor) radius.

For $\eta_e < 1$, the linear growth rate spectrum peaks at $k_y\rho_s < 1$, while a sharp transition to short wavelengths $k_y\rho_s > 2$ occurs for $\eta_e \gtrsim 1$. To determine whether Electron Temperature Gradient (ETG) driven modes are responsible for this sudden shift to short wavelengths at the $\eta_e = 1$ boundary, we created separate diagrams for modes having even and odd parities with respect to the midplane. For frequencies $\omega < \bar{\omega}_{be}$ (the average electron bounce frequency), trapped electrons will average odd parity potential fluctuations to zero. Therefore, odd parity modes cannot be driven by trapped electrons. However, ETG modes can be odd or even parity. We expect odd parity ETG modes to be only slightly weaker than even parity ETG modes as a result of more favorable average magnetic curvature and increased parallel Landau damping. However, we find odd parity modes much weaker than even parity modes in all cases, suggesting that trapped electrons are the main destabilizing influence in the parameter ranges considered. A comparison linear growth rates and frequencies from GS2, for even and odd parities, is shown in Fig. 2. Odd modes are very weak for $\eta_e < 1$, and weak for $\eta_e > 1$, suggesting that trapped electrons play a strong role even where ETG modes should be unstable for $\eta_e > 1$. Note that for $k_y\rho_s \gg 1$, the collisionless TEM becomes fluid-like (does not depend

on mode-particle resonances), and the most unstable modes propagate in the ion diamagnetic direction [11, 12, 13, 1]. We refer to this mode as the "ubiquitous mode" in Fig. 1.

Figure 3 shows the maximum linear growth rate from GS2 as a function of driving gradients. For $\eta_e < 1$, little change is seen in the k_y spectrum, and the growth rate is a function mainly of R/L_n. For $\eta_e > 1$, the growth rate increases strongly with R/L_{Te}. The growth rate spectrum remains relatively stationary for $\eta_e < 1$, as shown in Fig. 1.

We have compared the linear growth rate spectra from GEM and GS2 for both ITG and TEM cases. We obtained close agreement for the ITG case (not shown). The TEM case was compared for five different η_e values in Fig. 4. Results match within statistical errors, except at $\eta_e = 1.86$, for the largest k_y value from GEM. More detailed comparisons, perhaps using an 8-point rather than 4-point gyroaverage in GEM, will be pursued.

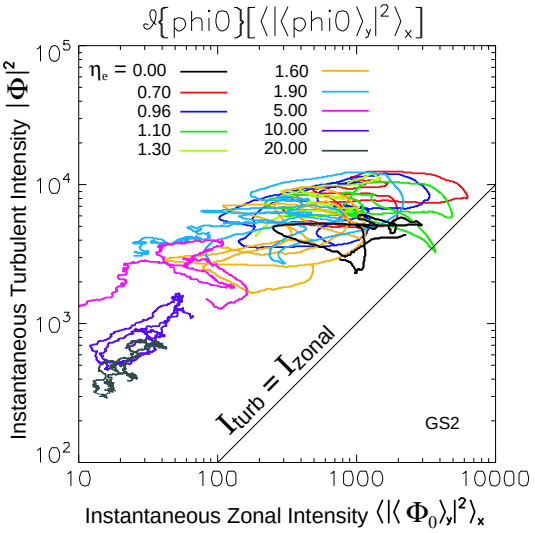

FIG. 6. Turbulent intensity vs. zonal flow intensity diverge as η_e increases, from GS2.

3. Nonlinear comparison of GEM and GS2 for TEM η_e scan

The sudden onset of short wavelengths in the linear GS2 studies when $\eta_e > 1$ suggests η_e may be an important parameter in nonlinear simulations of TEMs. This motivates us to consider a scan in η_e along a line normal to $\eta_e = 1$, to search for critical behavior as $\eta_e = 1$ is crossed. We have chosen to strongly drive TEMs by intersecting $\eta_e = 1$ at $(R/L_{Te}, R/L_n) = (10, 10)$, so that $R/L_n = 20 - R/L_{Te} = 20/(1+\eta_e)$, to avoid the nonlinear upshift regime [1, 2]. Values chosen for η_e are indicated by the black dots in Fig. 1.

Nonlinear runs were carried out using both GEM and GS2 flux tube simulations at ten values of η_e. For GEM, a real-space code, the box size was $45 \times 90\ \rho_s$, with $256 \times 128 \times 32$ spatial gridpoints in the (x, y, z) directions, and 64 particles per cell. For GS2, pseudo-spectral in the binormal direction, 11 k_y values were used with $k_y\rho_s = 0.0, 0.2, 0.4, \ldots, 2.0$, 85 $k_x\rho_s$ values were used, ranging from -10.5 to 10.5, for an equivalent box size $50 \times 62\ \rho_s$, while the nonlinear terms were evaluated using $128 \times 32 \times 32$ spatial gridpoints. GS2 runs used 16 energies and 32 pitch angles, with two signs of velocity.

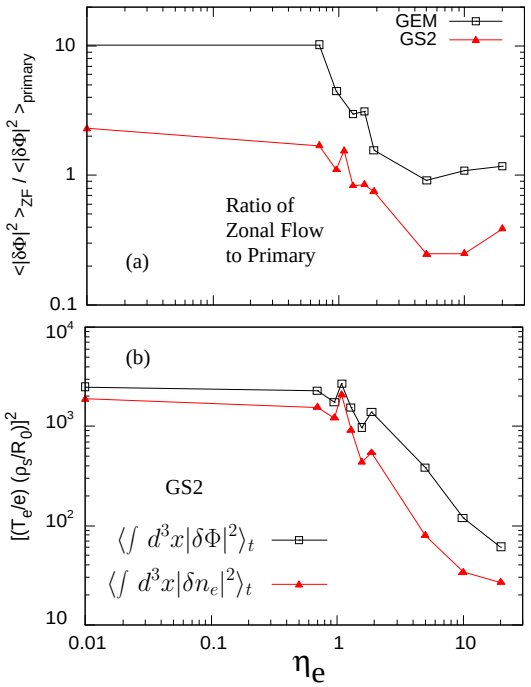

FIG. 7. (a) Ratio of time averaged squared potential for zonal flows to that of dominant primary mode, from GEM and GS2, drop sharply above $\eta_e = 1$. (b)Potential and density fluctuation level from GS2 drop exponentially for $\eta_e > 1$.

Comparison of the fluxes as a function of η_e is shown in Fig. 5. All of the time-averaged fluxes from the two codes very closely agree for $\eta_e < 2$. Relatively small departures can be seen

in the particle and ion thermal energy fluxes the three highest η_e values. The agreement in electron thermal energy flux is less impressive at the three highest η_e values. Ongoing work will attempt to understand this departure, which could be related to the difference in resolution in the *y*-direction.

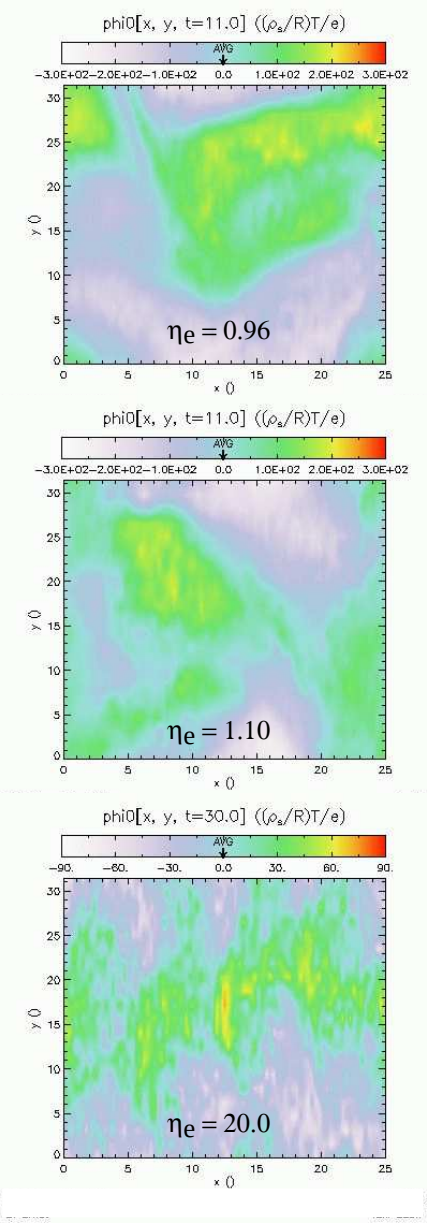

FIG. 8. Instantaneous contours of electrostatic potential in the first quadrant, vs. binormal coordinates (x,y) reveal fine scale radial structure superimposed on larger scales for $\eta_e = 20$. Contours from GEM appear remarkably similar for this case.

It is clear from Fig. 5 that η_e is an important parameter in nonlinear simulations. The variation with η_e mirrors changes in the linear wavenumber spectrum. For $\eta_e < 1$, little variation in fluxes is observed, particularly for particle and ion thermal fluxes. All three fluxes fall sharply and exponentially with η_e when $\eta_e > 1$. For $\eta_e = 20$, the fluxes have fallen two orders of magnitude.

4. Role of Zonal Flows as a Function of η_e

It has been established that zonal flows are unimportant in TEM saturation at large electron temperature gradients, and are the dominant saturation mechanism in purely density gradient driven cases. However, no explanation for this dependence on plasma parameters has been previously suggested. Here we demonstrate that the role of zonal flows, as well as the transport, in TEM turbulence is sensitive to η_e. Further, as in the linear studies, $\eta_e = 1$ is a critical value, above which zonal flows are relatively unimportant. This suggests, despite little resemblance between the nonlinear and linear wavelength spectra, that the shift of the linear TEM growth rate spectrum to short wavelengths for $\eta_e > 1$ strongly affects the role of zonal flows in TEM saturation.

Figure 6 shows the instantaneous turbulent intensity of electrostatic potential fluctuations vs instantaneous zonal intensity. Trajectories are traced as a function of time in the simulations. As η_e increases above unity, the trajectories move farther from the line of equality, suggesting that zonal flows play a much weaker role. In fact, the time-averaged ratio of zonal flow intensity to the intensity of the time-averaged dominant mode intensity from GS2 and GEM fall sharply above $\eta_e = 1$, as shown in Fig. 7(a). At $\eta_e = 5$, this ratio is an order of magnitude smaller. This remains true even though the total time-averaged squared potential and density fluctuations fall exponentially with η_e, as shown in Fig. 7(b). Note that Fig. 7(a) is a only qualitative comparison of GEM and GS2. The spectral densities are not corrected for their differing Jacobians. Nevertheless, the qualitative behavior of GS2 and GEM is remarkably similar.

At the largest η_e values, very fine scale radial structures appear, superimposed on larger scales, again consistent with expectation from the linear behavior. This is evident in the contour plots of turbulent potential from GS2 for $\eta_e = 20$ in Fig. 8, shown

in the binormal plane. The same contours from GEM appear nearly identical for the $\eta_e = 20$ case. Radial correlation functions from GS2 are shown in Fig. 9. For the largest values of $\eta_e = 10, 20$, very fine scale radial structure is clearly evident. This suggests that the nonlinear interaction may be viewed as a two-scale problem in which the fine scales give rise to an effective anomalous dissipation for the larger scales, leading to either direct saturation of the larger scales, or zonal flow damping and saturation by excitation of zonal density fluctuations. Following a similar line of reasoning, but treating the problem as a renormalized continuum of scales, a recent model suggests that TEMs saturate as a result of their own particle diffusivity [14], vaguely resembling an earlier model in which TEMs were suggested to saturate as a result of their own thermal conductivity [15] (see Eq. (4)). These models do not address zonal flow damping or the parametric dependence of zonal flows, and do not explain why zonal flows are found to be unimportant in the regimes considered. Our results suggest that a two scale model of zonal flow damping may be reasonable for $\eta_e \gg 1$. Negative correlations are also seen and are clear evidence of radial propagation at lower values of η_e, while the zonal modes are stationary at higher values of η_e. This differs markedly from the ITG case.

We have used the analysis package GKV to carry out bispectral analysis of the $\eta_e = 20$ case. Figure 10(a) shows the spectral density from GS2 as a function of frequency ω and poloidal wavenumber k_y, leading us identify the dominant primary mode with $\omega = \pm 1$ and $k_y = \mp 0.2$. The spectrum remains anisotropic in (k_x, k_y), consistent with the weak zonal flows, as shown in Fig. 10(b). The bicoherence (c) of $\delta\Phi(k_{x1} = 0, k_{y1} = 0.2)$, the dominant primary, $\delta\Phi(k_{x3} = 1.0, k_{y3} = 0.)$, the dominant primary after one poloidal transit, and $\delta\Phi(k_{x2} = 1, k_{y2} = 0.0)$, the zonal mode, reveals that the modes $\omega_1 = -1$ and $\omega_2 = 0$ are phase-locked. Accordingly, the dominant primary beats against itself, after one poloidal transit, to generate a stationary zonal mode at $(\omega_1 - \omega_1 = \omega_3 = 0, k_{x3} = 1, k_{y3} = 0)$. This picture supports the model proposed in Ref. [9], and may be related to ideas put forth in Refs. [16, 17, 18]. The interaction is shown in the inset diagram in Fig. 10(c). Note that $k_x = \hat{s}\theta k_y$, where $\hat{s} = 0.8$, so that after one poloidal transit, the $(k_x = 0, k_y = 0.2)$ mode corresponds to $(k_x = 2\pi\hat{s}k_y = 1.0, k_y = 0.2)$.

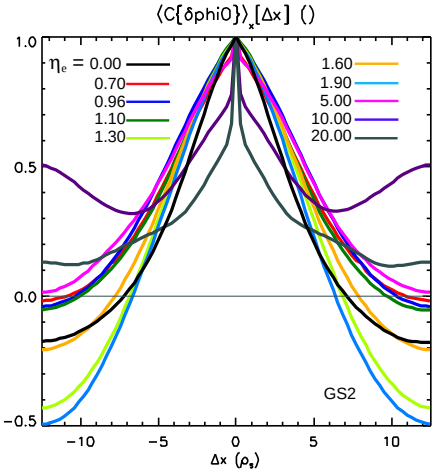

FIG. 9. Radial correlation functions from GS2. Very fine and very large scales co-exist for $\eta_e = 10, 20$.

The time-averaged nonlinear wavenumber spectra are compared in Fig. 11. This comparison can only be qualitative due to the different spectral densities of states in the two codes. However, GS2 and GEM display similar behavior, with the GS2 k_y spectrum narrowing much more strongly at the two largest η_e values. Most significant is the clear evidence of a subsidiary peak at $k_x = 1.0$ in both the GS2 and GEM spectra for $\eta_e = 20$, supporting the bicoherence analysis above.

5. Conclusion

We have developed a new linear stability diagram for electron modes as a function of electron temperature and density gradients, based on 2,000 gyrokinetic simulations, separating TEM, ubiquitous, and ETG modes. The most unstable wavenumbers transition sharply to short wavelengths for $\eta_e > 1$, which remain primarily destabilized by trapped electrons. This motivates us to investigate variation of zonal flows and transport with η_e in a series of nonlinear simulations

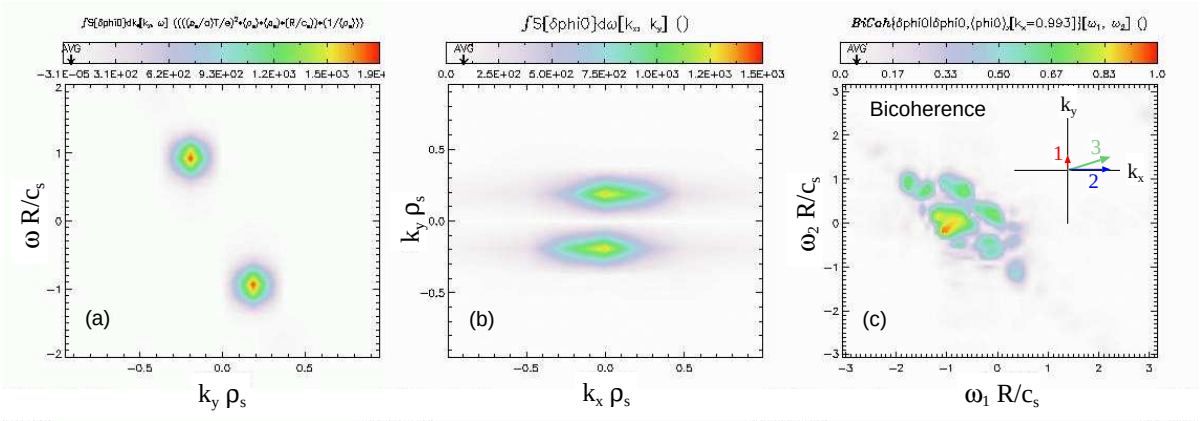

FIG. 10. GS2 results at $\eta_e = 20$: (a) Dispersion relation from nonlinear simulation shows the dominant mode is $\omega = \pm 1$, $k_y = \mp 0.2$, (b) Poloidal vs. radial wavenumber spectrum shows significant anisotropy, and (c) bicoherence of $(k_{x1} = 0, k_{y1} = 0.2)$ and $(k_{x2} = 1, k_{y2} = 0)$ reveals nearly perfect correlation of $\omega_1 = -1$ and $\omega_2 = 0$.

using both particle-in-cell (the GEM code) and continuum (the GS2 code) methods. The two codes are shown to closely agree except at the largest values of $\eta_e = d\ln T_e/d\ln n_e \geq 5$, where qualitative agreement is found. In particular, both codes show nearly identical behavior of the ratio of zonal flow intensity to dominant primary intensity as a function of η_e. Both transport and zonal flows are shown to fall sharply and exponentially as η_e exceeds unity. Fine scale structure appears when $\eta_e \gtrsim 1$, consistent with linear expectations. For $\eta_e \gg 1$, bispectral analysis supports a simple analytic model in which the dominant primary mode couples to itself to drive stationary zonal fluctuations.

For very large η_e, when zonal flows are found to be unimportant, fine radial scale structures are superimposed on larger scales associated with the primary instability. This is consistent with the expectation of short wavelength activity seen in the linear growth rate spectrum. Further, viewed as a two-scale problem, the fine radial scales may induce an effective dissipation on the larger scales. Considered together with the parametric variation of the linear spectrum, this could help explain why zonal flows are weak for $\eta_e > 1$. The results are also consistent with the adiabaticity of the ions at short wavelengths, where the zonal flow potential $\langle\phi\rangle \sim \langle n\rangle/k_r^2\rho_s^2$ is weaker for a given density perturbation, and secondary instability growth rates are reduced or stable [19, 20]. Thus, even though an initial zonal flow would be almost completely undamped by collisions [21] for the $k_\perp\rho_i > 1$ typical of temperature gradient driven TEMs, zonal flows are not strongly driven. Zonal flow damping via momentum transport driven by the fine scales acting on the larger scales could explain the dramatically reduced zonal flow levels for $\eta_e > 1$, and will be addressed in further work. Finally, this work makes the important step of verifying particle-in-cell and continuum methods for TEM turbulence, a significant test of kinetic electron dynamics in the two codes.

Supported by U. S. DoE contracts DE-FG02-91ER-54108, DE-FC02-04ER54784, the SCIDAC Center for Plasma Edge Simulation, and the DoE SCIDAC Center for the Study of Plasma Microturbulence. Computer simulations using GS2 were carried out on the MIT PSFC Parallel Opteron/Infiniband Cluster and those using GEM were carried out on the Cray XT4 machine Franklin at the DoE National Energy Research Supercomputer Center.

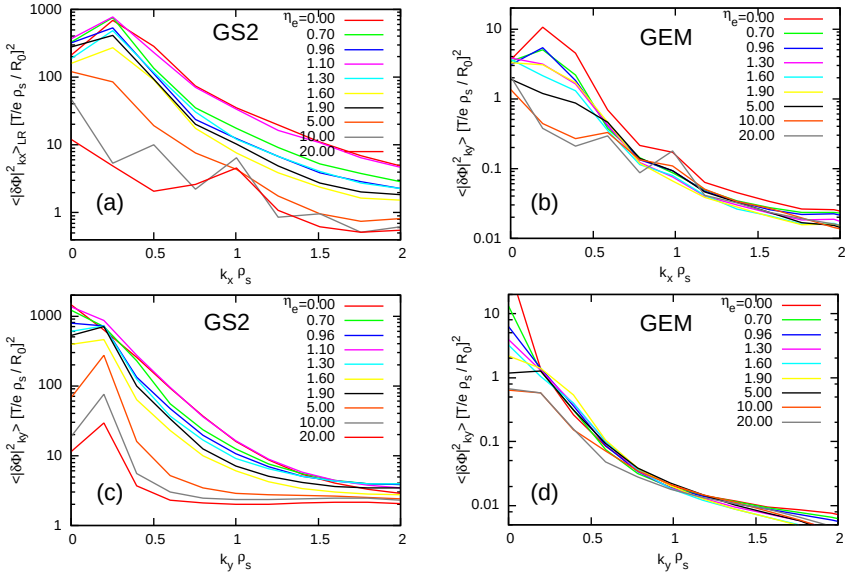

FIG. 11. Time averaged wavenumber spectra: (a) GS2 k_x spectrum shows dominant primary extends beyond one poloidal period in $\eta_e = 20$ case (subsidiary peak at $k_x\rho_s = 1$), (b) similarly for GEM k_x spectrum. (c, d) GS2 and GEM k_y spectra are qualitatively similar, with GS2 showing stronger variation at largest η_e values.

References

[1] ERNST, D. R. et al., Phys. Plasmas **11** (2004) 2637.

[2] ERNST, D. R. et al., in *Proc. 21st Int'l. Atomic Energy Agency Fusion Energy Conference, Chengdu, China, 2006*, IAEA-CN-149/TH/1-3. Available as `http://www-pub.iaea.org/MTCD/Meetings/FEC2006/th_1-3.pdf`.

[3] ANGIONI, C. et al., Phys. Plasmas **14** (2008) 055905.

[4] RHODES, T. et al., Plasma Phys. Contr. Fusion **49** (2007) B183.

[5] ERNST, D. R. et al., submitted to *Phys. Rev. Lett.*

[6] DANNERT, T. et al., Phys. Plasmas **12** (2005) 072309.

[7] LANG, J. et al., Phys. Plasmas **14** (2007) 082315.

[8] HOFFMAN, M. et al., Bull. Am. Phys. Soc. (2007).

[9] LANG, J. et al., Phys. Plasmas **15** (2008) 055907.

[10] DIMITS, A. M. et al., Phys. Plasmas **7** (2000) 969.

[11] COPPI, B. et al., Nucl. Fusion **17** (1977) 969.

[12] COPPI, B. et al., Phys. Rev. Lett. **33** (1974) 1329.

[13] COPPI, B. et al., **2** (1990) 2322.

[14] MERZ, F. et al., Phys. Rev. Lett. **100** (2008) 035005.

[15] LI, J. et al., Plasma Physics Control. Fusion **44** (2002) A479.

[16] CHEN, L. et al., Phys. Plasmas **7** (2000) 3129.

[17] TERRY, P. W. et al., Phys. Rev. Lett. (2002).

[18] GATTO, R. et al., Phys. Plasmas **13** (2006) 022306.

[19] DORLAND, W. D. et al., Phys. Rev. Lett. **85** (2000) 5579.

[20] ROGERS, B. N. et al., Phys. Rev. Lett. **85** (2000) 5336.

[21] XIAO, Y. et al., Phys. Plasmas **13** (2006) 102311.